ORNL/SPR-2021/2096
Rev. 0

Modifications to MiniFuel Vehicle to Enable Higher Temperature UO_2 Irradiation Capabilities

Nuclear Technology Research and Development

Prepared for
U.S. Department of Energy
Nuclear Technology R&D Program
Advanced Fuels Campaign

Authors:
Jacob P. Gorton, Zane G. Wallen, Christian M. Petrie
Oak Ridge National Laboratory

August 2021
M2FT-21OR020203043

ACKNOWLEDGEMENTS

This research was sponsored by the Advanced Fuels Campaign (AFC) Program of the US Department of Energy (DOE), Office of Nuclear Energy. Neutron irradiation in the High Flux Isotope Reactor (HFIR) is made possible by the Office of Basic Energy Sciences, US DOE. The report was authored by UT-Battelle under Contract No. DE-AC05-00OR22725 with DOE. Heath McCartney compiled the engineering drawings of the modified irradiation vehicle design. Ryan Gallagher and Kory Linton performed technical reviews of this report.

SUMMARY

The Advanced Fuels Campaign (AFC) within the US Department of Energy Office of Nuclear Energy (DOE-NE) supported the conception and initial demonstration of the miniature fuel (MiniFuel) irradiation capability in the High Flux Isotope Reactor (HFIR) at Oak Ridge National Laboratory. These MiniFuel experiments are a key component of a larger effort to accelerate the qualification of novel fuel concepts and to reduce uncertainty in fuel performance models. MiniFuel experiments to date have been conducted in HFIR's outer vertical experimental facility (VXF) positions. However, there is motivation to achieve irradiation temperatures and fuel burnup accumulation rates greater than what is achievable in the VXF positions to explore high-temperature phenomena and further accelerate fuel qualification. Therefore, MiniFuel irradiation experiments are being considered in HFIR's removable beryllium region, which is closer to the fueled core than the VXF region. This report summarizes the design modifications to the MiniFuel irradiation vehicle needed to enable high-temperature (i.e., >1,000°C) irradiation tests with rapid burnup accumulation.

CONTENTS

ACKNOWLEDGEMENTS i

SUMMARY ii

FIGURES i

TABLES ii

1. INTRODUCTION 1

2. METHODOLOGY 2
   - 2.1 Geometric Modifications to the MiniFuel Irradiation Vehicle 2
   - 2.2 Neutronic Analysis 3
   - 2.3 Thermal Hydraulic Analysis 3
   - 2.4 Finite Element Thermal Analysis 5

3. RESULTS 7
   - 3.1 Neutronic Results 7
   - 3.2 Thermal Hydraulic Results 10
   - 3.3 Thermal Analysis 11

4. SUMMARY AND CONCLUSIONS 15

5. REFERENCES 16

FIGURES

Figure 1. RB irradiation vehicle. 2

Figure 2. Nodalization diagram for MiniFuel basket RELAP5-3D model. 4

Figure 3. Quarter symmetry target model. 6

Figure 4. Gamma heating in nonfuel components in the sub-capsules with the highest and lowest HGRs. 7

Figure 5. Axial distribution of gamma HGRs in nonfuel components at BOC, MOC, and EOC in the radial position nearest to HFIR's core. 8

Figure 6. Fission and gamma heating in fuel specimens in the sub-capsules with the highest and lowest HGRs. 8

Figure 7. Axial distribution of HGRs in fuel specimens at BOC, MOC, and EOC in the radial position nearest to HFIR's core. 9

Figure 8. Fuel fission HGR and burnup in the RB and VXF positions for the fuel specimen nearest to HFIR's core 9

Figure 9. Histogram of mass flow rates predicted through the RB MiniFuel experiment for the range of possible basket and target geometries. 10

Figure 10. Distribution of predicted HTCs for each axial target position separately (*top*) and lumped together (*bottom*). 11

Figure 11. Temperature distribution for target internals for position 12 at EOC 4. 13

Figure 12. Predicted fuel temperatures in target position 12 as a function of irradiation time. Markers represent average values and error bars represent the minimum to maximum range. 14

Figure 13. Predicted fuel temperatures in target position 32 as a function of irradiation time. Markers represent average values and error bars represent the minimum to maximum range. 14

Figure 14. Spatial ΔT in target position 12 as a function of irradiation time. S indicates sub-capsule position. 15

TABLES

Table 1. Example MiniFuel test matrix. 11
Table 2. Target design parameters that meet example design goals. 12

MODIFICATIONS TO MINIFUEL VEHICLE TO ENABLE HIGHER TEMPERATURE UO_2 IRRADIATION CAPABILITIES

1. INTRODUCTION

Novel nuclear fuel concepts must undergo irradiation testing as part of the qualification process for eventual deployment. Historically, the fuel qualification process has relied heavily on performing many integral tests in which nuclear fuels are subjected to expected operational conditions in their prototypic geometric form [1]. A prominent challenge associated with this approach is that numerous independent variables affect performance and safety characteristics of nuclear fuels that are unable to be tightly controlled during integral fuel testing. In addition, executing these integral tests generally requires large, complex experiment designs that are specific to a narrow range of fuel parameters and operational conditions for the intended application. The inability to control each independent variable leads to an extensive and costly test matrix in terms of capital and time and to large uncertainties in fuel performance models. These costs can become prohibitive and stifle innovation in new fuel concepts or in extending existing fuel concepts to a wider range of applications (e.g., operating temperature, burnup, or power density). To mitigate these challenges and accelerate qualifying new nuclear fuel concepts, a complimentary separate effects irradiation approach has been proposed in coordination with integral effects tests. This approach will isolate key variables that have the greatest impact on the progression of fuel performance throughout its operational lifetime [2]. The testing of miniature fuel (MiniFuel) specimens in the High Flux Isotope Reactor (HFIR) at Oak Ridge National Laboratory has been a successful example of separate effects testing in which the size of fuel specimens was reduced to minimize fuel temperature gradients and ensure that most of the heat produced in the irradiation sub-capsules is generated through gamma heating [3]. This approach effectively makes the fuel temperature independent from the fuel specimen fission rate, thus allowing for a nearly constant temporal fuel temperature with accelerated burnup and the flexibility to test many different fuel forms without significant changes to the irradiation vehicle.

The first MiniFuel irradiation assembly was inserted into one of HFIR's Vertical Experiment Facilities (VXF) in June 2018 and demonstrated the capability to perform a nearly isothermal irradiation test with accelerated burnup accumulation and fuel temperatures held in the vicinity of 450°C–550°C [3, 4]. Since that time, additional MiniFuel experiments have been initiated [5, 6, 7], but almost all these tests have been limited to temperatures <900°C. For fuels such as uranium dioxide (UO_2), it has been shown that irradiation temperatures beyond 1,000°C are necessary to observe significant fission gas release for moderate burnups in the range of 40–50 MWd/kg-U [8]. The current work seeks to expand the MiniFuel capability by modifying the irradiation vehicle to perform testing in HFIR's removable beryllium (RB) reflector region. Irradiation in the RB positions, which are closer to HFIR's core compared with the VXF positions, will result in higher gamma and neutron fluence rates, and therefore higher heat generation rates (HGRs) in the fuel specimens and sub-capsule components. Three primary motivating factors exist for expanding the MiniFuel separate effects-testing capabilities to the RB positions: (1) the greater HGRs will enable high-temperature (i.e., >1,000°C) testing;(2) burnup accumulation will occur more rapidly than in the VXF positions, allowing for a faster turnaround when screening new fuel concepts; and (3) expansion to the RB region will increase the experiment throughput by opening additional testing positions in HFIR. This report details the design changes to the MiniFuel irradiation vehicle needed to enable testing in HFIR's RB positions and provides initial neutronic and thermal analyses of the modified design concept. Sensitivity

analysis, machine learning, and optimization techniques are used to design an experiment based on a preliminary test matrix that demonstrates the range and flexibility of the MiniFuel RB design.

2. METHODOLOGY

2.1 Geometric Modifications to the MiniFuel Irradiation Vehicle

The irradiation vehicle used for the VXF MiniFuel experiments consisted of a basket assembly that could hold up to nine target assemblies. Each target contained six individually sealed sub-capsules, and the nine targets were arranged in three radial and three axial positions in the basket assembly. The basket design concept being considered for irradiation in the RB positions is based on a previous capsule-holder design that was developed several decades ago, but the design was modified so the VXF target design is compatible with the RB basket assembly. Reusing the target design greatly simplifies the design process since the engineering drawings already exist and experience building the targets has already been acquired. A key difference between the VXF basket assembly and the modified RB basket is that the latter has five radial positions and can therefore hold up to 15 targets, compared with 9 targets in the VXF basket assembly.

Figure 1 shows three-dimensional (3D) models of the basket, target, and sub-capsule assembly models. HFIR's RB positions have an aluminum liner in which the basket assembly will be seated. Target locations can be identified by a radial and axial (RA) identifier, and a specific sub-capsule location can be identified by a radial, axial, and sub-capsule (RAS) identifier. The numeric identifiers are called out in Figure 1. The outer surface of the target assemblies will be exposed directly to HFIR's coolant, which flows downward over the irradiation positions at ~50–60°C. A thimble is situated in between each sub-capsule to keep them centered within the target housing, and two compression springs are used at the axial ends of each target to keep the stack of sub-capsules in contact. Within each sub-capsule holder is a filler tube, silicon carbide thermometry, cup, fuel specimen, grafoil insulators, and an end cap. The holder, filler tube, and cup are all made of molybdenum, a refractory metal with high density, high melting point, high thermal conductivity, high photon heat generation rate, and low chemical reactivity. The target housing is made of stainless steel and the basket is made of aluminum 6061. For this initial design report, the fuel considered is a 3-mm diameter disk with variable thickness.

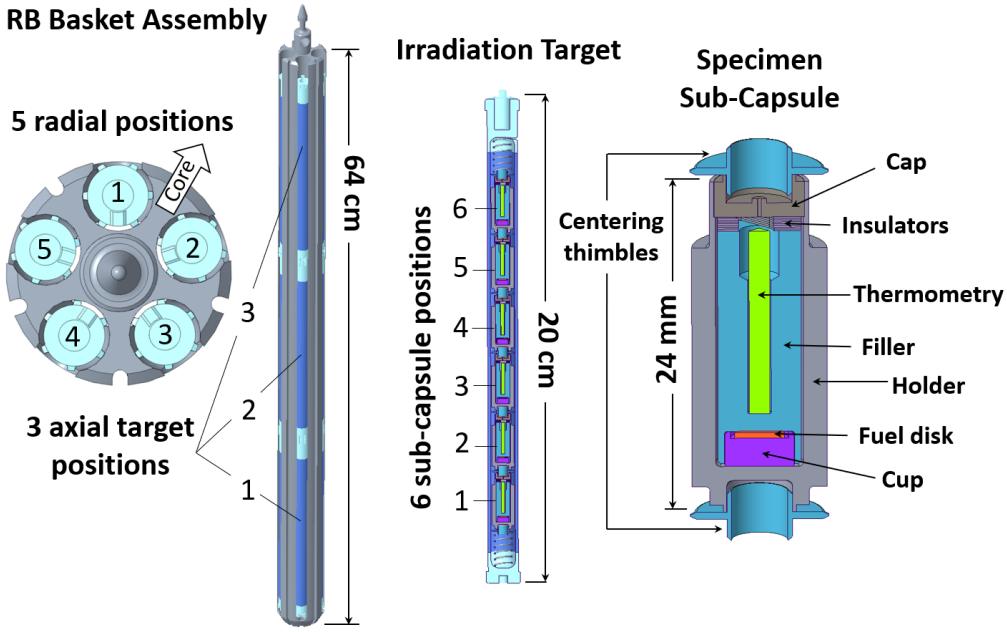

Figure 1. RB irradiation vehicle.

Each target is filled with an inert gas of either helium or a helium/argon mixture. Ideally, the majority of nuclear heating produced inside each sub-capsule is generated from gamma heating in the nonfuel components, as opposed to fission heating in the fuel. This reduces the sensitivity of the fuel temperature to changes in fission heating with increasing with burnup. The fuel temperature is controlled primarily by the thickness of the fuel disk, the gas gap between the sub-capsule holder and the target housing, and the inert target fill gas composition. A primary contribution of this report is applying sensitivity analysis methods and machine learning algorithms to optimize these variable parameters to reach an initial representative set of design goals.

2.2 Neutronic Analysis

Monte Carlo neutronics methods were used to calculate neutron and photon heating in all target components in all 15 target positions for a preliminary basket design. These calculations were performed using a version of the MCNP5 Monte Carlo neutronics code [9], the SCALE software package [10], and the ADVANTG [11] variance-reduction tool that are coupled together using a wrapper code called HFIRCON [12]. Beginning and end-of-cycle MCNP models of HFIR cycle 400 (April 27, 2004–May 21, 2004) [13] were modified to include the preliminary basket assembly design in an RB position and used for the neutron and photon heating, fission rate, and fuel burnup as a function of irradiation time in HFIR. The HFIRCON wrapper automates a five-step process that accounts for heating from prompt- and delayed-fission neutrons, prompt-fission photons, fission product decay photons, local α and β heating, and photon emission from activated materials. The HFIRCON algorithm can be described by the following five steps:

1. Run the MCNP HFIR model to acquire prompt neutron and photon heating and the neutron flux spectrum.
2. Run another MCNP model to calculate fission product heating based on a fixed-photon source defined by the accumulation of fission products throughout the core.
3. Input the neutron flux spectrum calculated in Step 1 into the COUPLE module within the SCALE framework to calculate problem-specific cross section data which are then used by the SCALE ORIGEN module to calculate α and β decay heating and the gamma flux spectrum within activated components.
4. Input the gamma flux spectrum into a third MCNP model to calculate the activation product heating.
5. Update the MCNP model with isotopic compositions determined during the ORIGEN calculation to allow for multicycle calculations.

ADVANTG is used in the MCNP calculations to implement variance reduction techniques to minimize the required number of source particle histories to simulate and therefore reduce the run time while still obtaining statistically reliable results. This calculation procedure is consistent with previous MiniFuel calculations performed for VXF experiments [3].

For this initial design activity, all fuel specimens were assumed to be natural (0.71 wt %) enriched UO_2, and four HFIR cycles, each 26 days, were simulated with 25 days of downtime assumed between cycles. Heating rates in W/g were calculated for all target and sub-capsule components for all 15 positions. Values for the heating rates in the aluminum components (i.e., the liner and the basket) and direct energy deposition in the coolant were assumed to be equivalent to values predicted in a previous HFIR safety calculation for an experiment in an RB position.

2.3 Thermal Hydraulic Analysis

A thermal hydraulic model of the MiniFuel RB basket assembly was developed in RELAP5-3D [13] to calculate the coolant mass flow rate through the experiment and to determine the heat transfer coefficient (HTC) between the target housing and coolant. The HTC was later used in the convective boundary condition in the finite element (FE) thermal model of a single target described in Section 2.4. The RELAP model consists of an inlet time-dependent volume that flows into the open top of the liner above the basket

assembly, after which a multijunction splits the flow into two separate channels. One channel is in between the RB liner and the outer diameter of the basket assembly, and the other channel is a lumped flow path of the five target holder slots within the basket. These channels were modeled as two "pipe" components in RELAP with crossflow modeled between the pipes. The basket, the 15 targets, and the liner were modeled as three heat structures. By separating the flow paths and heat structures in this fashion, the HTC between the targets and the surrounding coolant could be isolated. A nodalization diagram of the RELAP5-3D model is shown in Figure 2 with numeric volume identifiers. Notably, the basket and liner heat structures extend the entire length of the basket assembly, whereas the target heat structure only extends a portion of the total length to match the few centimeters of empty space in the basket assembly above the targets. There is also approximately 0.5 centimeter of empty space below the targets caused by a dimensional change at the bottom of the radial positions in the basket.

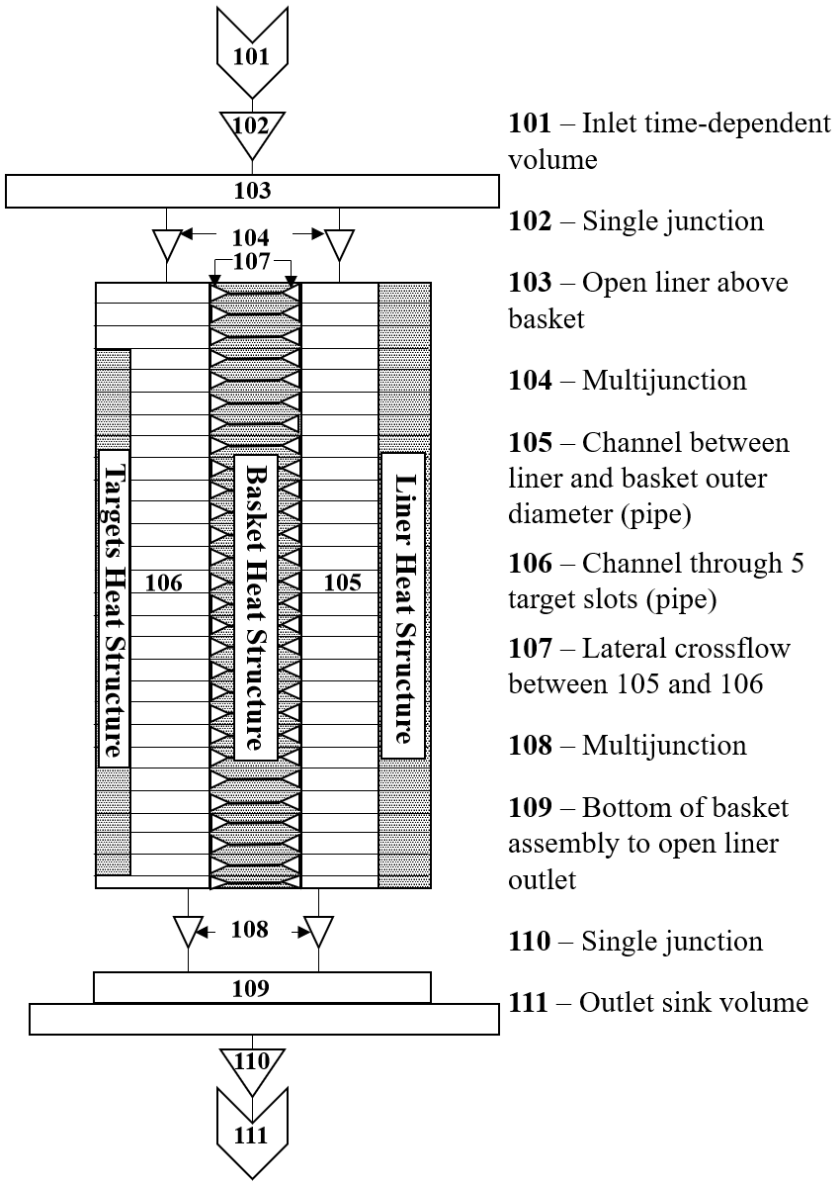

Figure 2. Nodalization diagram for MiniFuel basket RELAP5-3D model.

The total power applied to the model summed to approximately 45.7 kW and accounted for the heat generated in the targets at each of the 15 positions calculated using HFIRCON, as well as the gamma heating

in the liner, basket, and coolant based on heating rates in aluminum and water calculated in a previous report. Although the capsule design in the reference calculation differed from the MiniFuel basket design, the nonpublic calculation showed that the HGRs in the liner and capsule were equivalent despite their differing geometries. That same assumption is applied here since the reference capsule and MiniFuel basket are both aluminum. The radial dependence of power in the targets is inherently ignored by lumping all radial target positions into a single heat structure, and the axial dependence of power was also ignored (i.e., a uniform axial power profile was assumed in all heat structures). These assumptions have little impact on HTC calculations because the underlying heat transfer equations used for predicting the HTC are functions of the basket geometry, flow conditions, and coolant thermal properties. Typical coolant flow rates through a HFIR RB experiment are such that the expected coolant temperature rise is less than 10°C. It is therefore reasonable to use the Dittus-Boelter approximation for single-phase heat transfer [14] with constant water thermal properties, which is independent of local power.

The pressure drop across the RB reflector was calculated to be approximately 10 psi in a previous report. The mass flow rate through the experiment was calculated in this analysis by setting the pressure drop across the entire length of the model to 10 psi and then using a controller variable within RELAP to calculate the coolant mass flow rate required to achieve that pressure drop. RELAP calculates the pressure drop as a sum of losses due to acceleration, gravity, and friction. Form loss coefficients were included in the model to account for momentum losses that occur at sudden cross-sectional flow area changes, including when the coolant flows from the open liner into the top of the basket assembly, coolant inside the five target holder channels reaches the top of the targets, and the flow exits the basket assembly into the open liner. Frictional losses in the model depend on the Reynolds number, which in turn depends on the hydraulic diameter in the pipes. The greatest contributor to friction and pressure losses in the model is flow around the targets, owing to the relatively small hydraulic diameter between the targets' outer walls and the holder slots in the basket.

Sensitivity analysis methods were applied to the RELAP model to determine the impact of geometric tolerances of the assembly components on the mass flow rate and HTC. Geometric tolerances of the various assembly dimensions were assumed to be equivalent to the tolerances given on the existing engineering drawings, which the modified MiniFuel basket was based on. A Python script was developed to randomly sample the various dimensions (primarily diameters and lengths) within their tolerances and then calculate the cross-sectional flow areas, hydraulic diameters, lengths, heat transfer surface areas, and form loss coefficients required by the RELAP model. A template of the model was created, which the Python script would then auto-populate to generate a working RELAP input deck. This methodology was used to ensure that the mass flow rate was within acceptable limits from a HFIR safety perspective and to determine the potential range of HTCs that may need to be considered in the FE thermal model of a single target.

2.4 Finite Element Thermal Analysis

FE thermal analysis was performed using a quarter-symmetry model of a single MiniFuel target developed in the commercial FE software package ANSYS. The target model used was adapted from ANSYS models used in previous MiniFuel works [3, 15, 16] and used custom macro programs for calculating thermal contact conductance through variable gas gaps [17]. Temperature-dependent material properties were implemented for each of the nonfuel components, as previously described by Petrie et al. [3]. The thermal property files are maintained internally and have been reviewed for quality assurance. Temperature, theoretical density, and burnup-dependent properties were implemented for the UO_2 fuel disks [18, 19]. A theoretical density of 95% was assumed, and a Python script was used to read the fuel burnup predicted using HFIRCON into ANSYS. The Python script was also used to read heat generation rates for each target component based on the number of days and position in HFIR and set the internal heat generation in each component in the ANSYS model. A convective boundary condition was applied to the outer surface of the target housing using a bulk coolant temperature of 58°C (the average HFIR coolant temperature), and the HTC was set based on the results of the RELAP5-3D calculations described in Section 2.3. A mesh

refinement study was performed in which the element size in the fuel and all nonfuel components was reduced until predictions in maximum fuel temperature changed by less than 1°C. The resulting element sizes are 0.1 mm in the fuel disks and 0.5 mm in nonfuel components. Figure 3 shows the quarter-symmetry ANSYS model of the target.

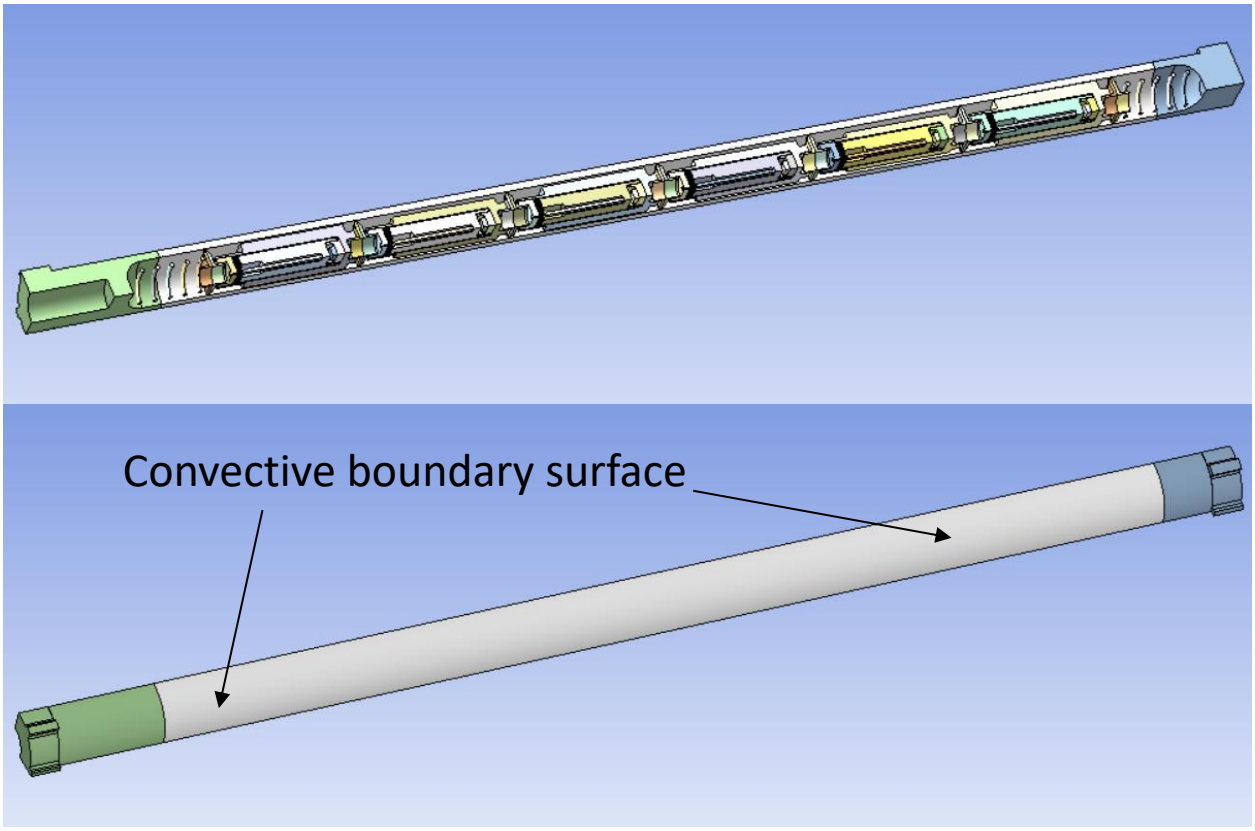

Figure 3. Quarter symmetry target model.

Parametric design and reduced-order modeling (ROM) techniques were applied to identify designs for meeting representative test matrix requirements. The key parameters that can be varied to achieve a suitable target design are the gas gap thickness between each sub-capsule and the target housing; the fill gas composition (helium, argon, or a mixture); the fuel disk thickness; and the radial and axial position of the target within the basket, which changes the heat generation rate within each target component. The parametric design studies also varied the number of days that the target has been irradiated in HFIR, which in turn impacts heat generation rates and the thermal conductivity of the fuel, which is both temperature and burnup dependent. An ideal design is one that meets a desired average fuel temperature (e.g., 1,000°C, 1,100°C, and 1,300°C, potentially all within a single target) while minimizing the spatial and temporal ΔT experienced in the fuel disk. Minimizing the fuel ΔT is an essential feature of MiniFuel tests because the primary goal of these experiments is to produce single-effects results in which the impact of a single independent variable, such as temperature and burnup, can be isolated.

3. RESULTS

3.1 Neutronic Results

For each 26 day irradiation cycle, HFIRCON simulations were performed at the start of the cycle (day 0) and on days 1, 3, 5, 10, 15, 20, 22, 24, and 26. The HGRs in fuel and nonfuel sub-capsule components vary significantly with the spatial location of the sub-capsule within the MiniFuel basket assembly. In a single sub-capsule, the nonfuel component that generates the most heat is the sub-capsule holder. Figure 4 shows the total capsules with the highest and lowest HGRs within the holder material (refer to Figure 1 for component designations) as a function of days in HFIR for the sub-capsule holders with the highest and lowest average HGR based on their location in the basket. Each data point on the figure corresponds to the days for which a HFIRCON calculation was performed. The total HGRs include prompt and delayed neutron and gamma heating, although HGRs in the holder material are attributed approximately 93–96% to gamma heating. The RAS positions corresponding to the highest and lowest holder HGRs shown in Figure 4 are 124 and 436, respectively. Figure 5 shows the axial variation in total gamma HGRs generated by the holder material at the beginning, middle, and end of the fourth HFIR cycle in the radial position nearest to HFIR's core. Together, Figures 4 and 5 show the variation of HGRs in the holder material due to spatial and temporal effects. Other sub-capsule materials generate less heat than the sub-capsule holder but experience similar relative spatial and temporal HGR variations.

Figures 6 and 7 show similar distributions of the total HGR from fission and gamma heating in the fuel specimens. In Figure 6, the total HGR as a function of time is shown for the fuel specimens with the highest and lowest total HGRs on average, which occur in RAS positions 124 and 111, respectively. The gaps between data points occurring from 27–51 days, 78–102 days, and 130–154 days in Figures 4 and 6 correspond to reactor downtime between the four cycles modeled in HFIRCON. Figures 4 and 6 also show a large increase in HGR between the first and second day of each HFIR cycle, which is caused by the movement of HFIR's control blades and the initial accumulation of fission products in the HFIR fuel. From the beginning of cycle (BOC) 4, to the middle of cycle (MOC) 4, to the end of cycle (EOC) 4, the HGRs in nonfuel components show an approximate 15%–22% increase, and the fuel specimens show a 30%–150% increase in HGR. The largest increases in fuel HGRs occur in the specimens in the highest and lowest axial positions.

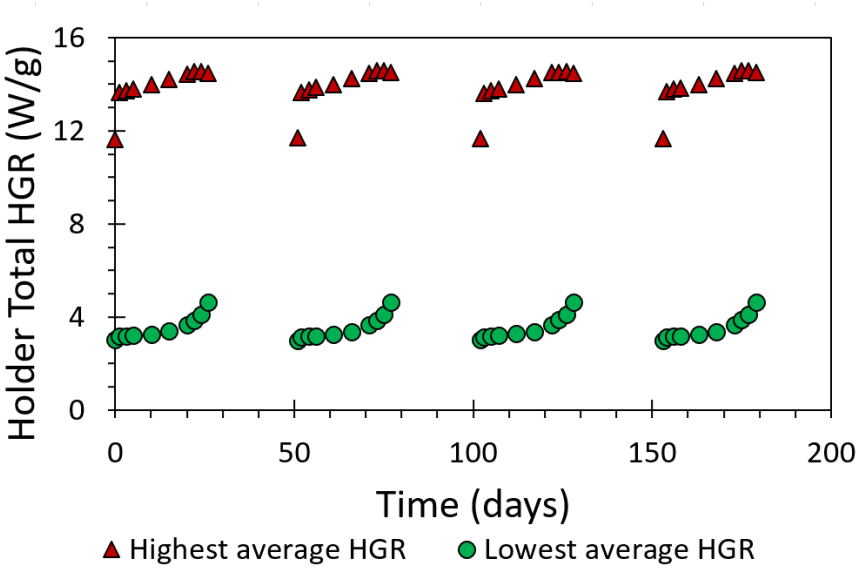

Figure 4. Total HGRs of the sub-capsule holders with the highest and lowest HGRs on average.

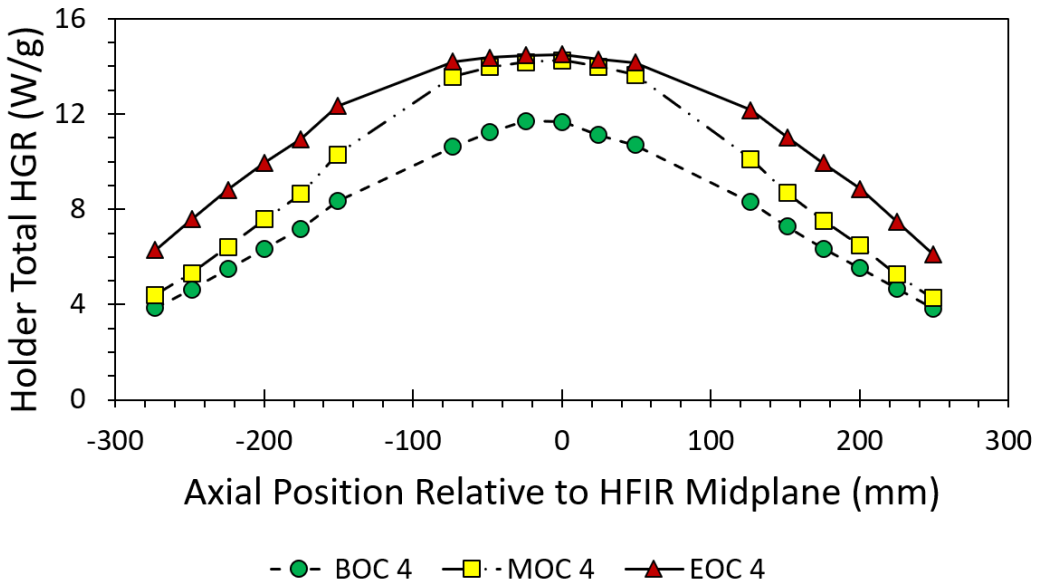

Figure 5. Axial distribution of HGRs in sub-capsule holders at BOC, MOC, and EOC in the radial position nearest to HFIR's core.

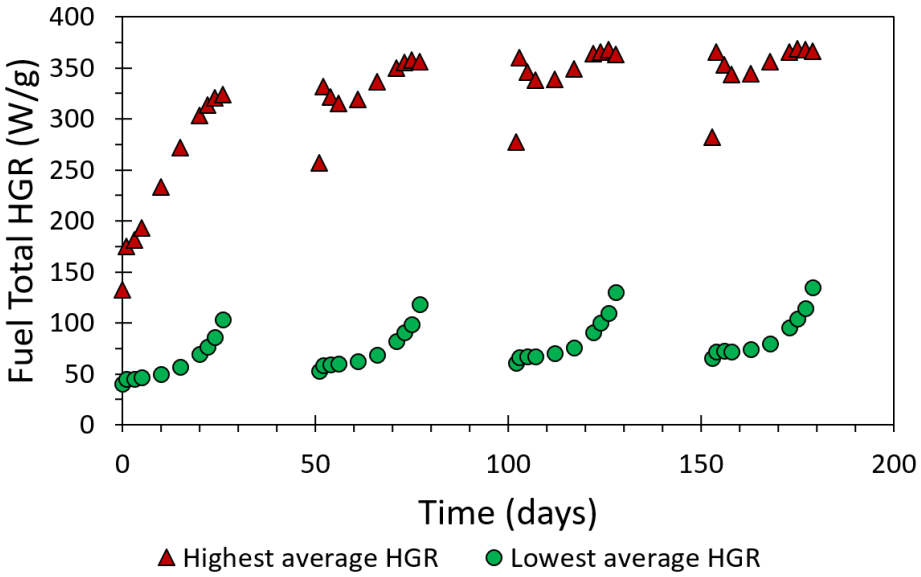

Figure 6. Total fission and gamma heating in the fuel specimens with the highest and lowest HGRs on average.

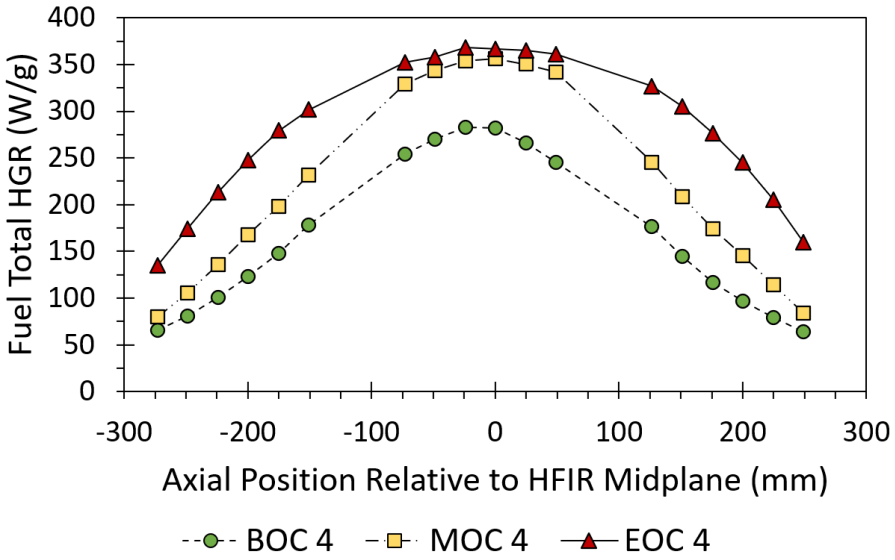

Figure 7. Axial distribution of HGRs in fuel specimens at BOC, MOC, and EOC in the radial position nearest to HFIR's core.

Figure 8 compares the fuel fission HGR only (gamma heating ignored) and burnup of natural UO_2 in the sub-capsule located nearest to HFIR's core in a VXF position [3] vs. the RB position. The RB data were adjusted to have 15 day downtimes between cycles to reflect the same reactor downtime assumed in previous VXF work. This adjustment has no impact on the burnup since burnup is not accumulated when the reactor is off. The figure shows that the fission HGR in the fuel reaches approximately 367 W/g in the RB position after the initial buildup of fission products and plutonium breeding that occur in the first two cycles, and the fission HGR in the VXF position reaches about 150 W/g. The fission HGR and burnup accumulation rate is approximately 2.25 times greater in the RB position compared with the VXF position.

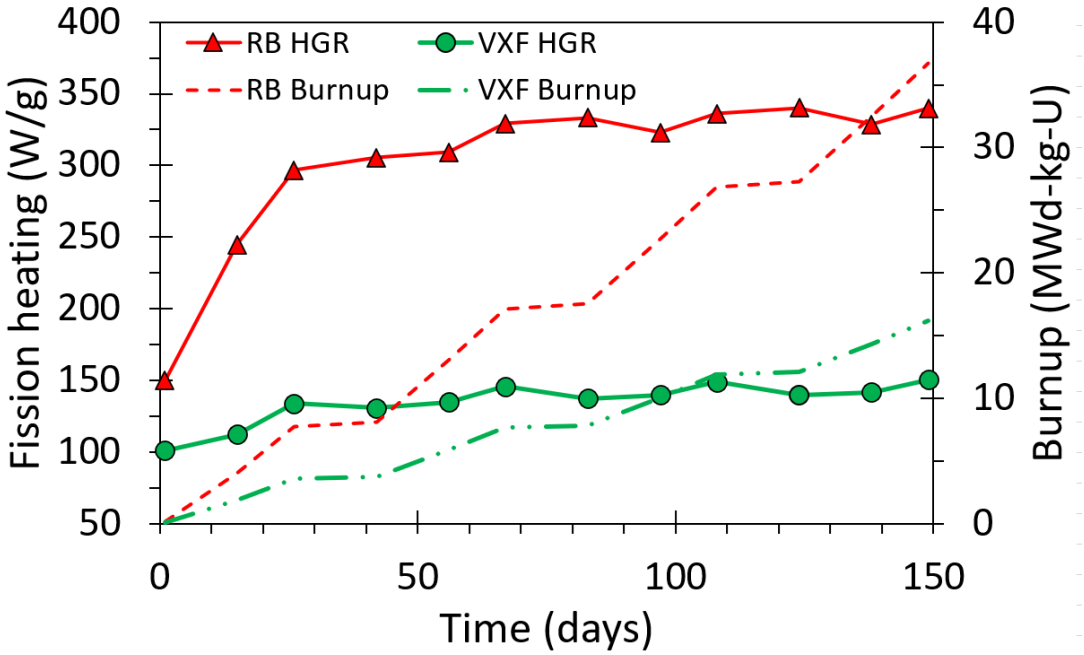

Figure 8. Fuel HGR from fission only and burnup in the RB and VXF positions for the fuel specimen nearest to HFIR's core.

3.2 Thermal Hydraulic Results

A total of 753 RELAP calculations were performed to determine the range of possible mass flow rates and target-to-coolant HTCs that could occur due to variations in the target and basket geometry. Of the 753 calculations, one used nominal dimensions for the basket and target, one used values that led to the minimum possible flow rate through the experiment, one used dimensions that led to the maximum possible flow rate, and the remaining 750 randomly sampled dimensions within the tolerances specified on engineering drawings. Figure 9 shows a histogram of the resulting mass flow rates through the MiniFuel experiment. The results from the nominal, minimum, and maximum flow area cases are specified on the figure, as is the minimum allowable mass flow rate according to a previous HFIR safety calculation. A relative margin of 8.1% exists between the minimum allowable mass flow rate limit of 1.123 kg/s and the minimum possible value of 1.214 kg/s. A maximum flow mass flow rate of 1.520 kg/s was predicted. Previous HFIR safety calculations have been approved that predicted mass flow rates as high as 1.7 kg/s through an RB experiment, providing evidence that this experiment will not divert too much flow from the HFIR fuel. The relative difference between the nominal flow rate value of 1.356 kg/s and the average value obtained from all 753 cases (1.358 kg/s) is 0.1%, and the range of the average value plus or minus 3 standard deviations approximately matches the minimum and maximum flow area cases. This observation indicates that a statistically reliable normal distribution of possible mass flow rates has been obtained.

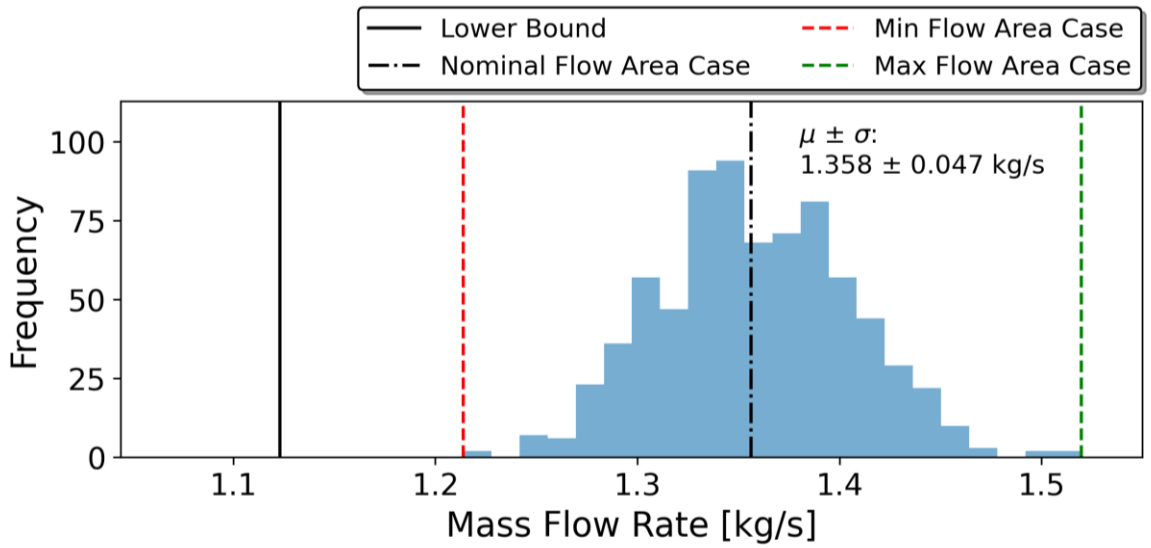

Figure 9. Histogram of mass flow rates predicted through the RB MiniFuel experiment for the range of possible basket and target geometries.

The range of HTCs at each of the three axial target positions was predicted for each of the 753 RELAP cases. Figure 10 shows the HTC distribution for all three axial positions separately and then for the three positions lumped together. The figure indicates a relatively small variation in HTC as a function of axial position and model geometry. The approximate average value from all three lumped positions of 22.5 kW/m^2-K was used as the nominal value in the ANSYS models.

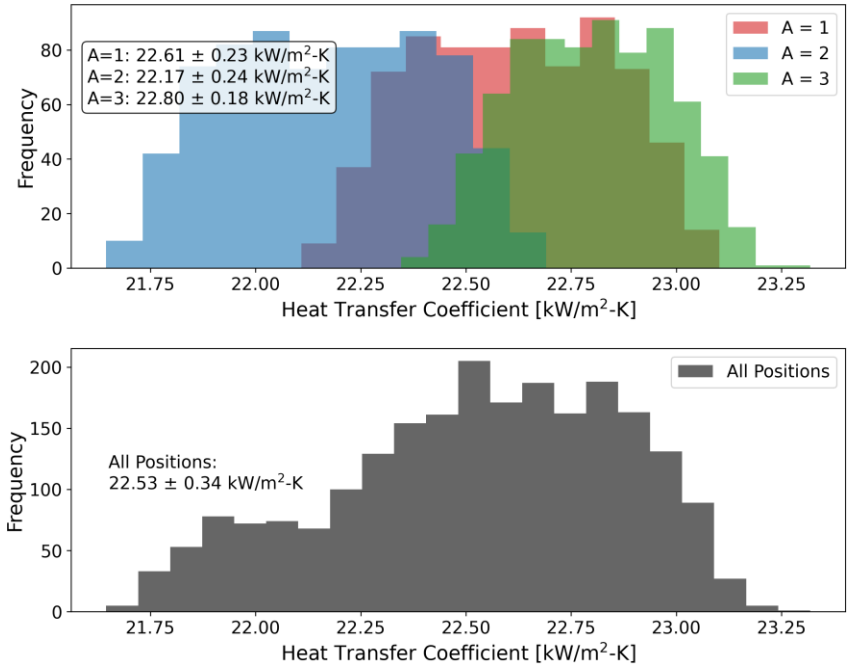

Figure 10. Distribution of predicted HTCs for each axial target position separately (*top*) and lumped together (*bottom*).

3.3 Thermal Analysis

Table 1 shows an initial test matrix for a future RB MiniFuel campaign targeting improved understanding of fission gas release in UO_2 as a function of temperature and burnup These goals are representative of MOC and EOC burnups and fuel centerline temperatures in light water reactors. In addition to the average temperature and discharge burnup goals listed in Table 1, maintaining a temporal and spatial ΔT that was as low as possible and preferably no more than 100°C was also desirable.

Table 1. Example MiniFuel test matrix.

Goal T_{avg} (°C)	Goal Burnup (MWd/kg-U)	Number of specimens
1,000	40	2
1,000	80	2
1,100	40	2
1,100	80	2
1,300	40	2
1,300	80	2

Through inspection of the burnup values predicted using HFIRCON, the authors found that radial and axial (RA) positions 12 and 32 (refer to Figure 1 for RA identifiers and position relative to HFIR's core) were the most suitable for achieving the desired discharge burnups in as few irradiation cycles as possible. The

six fuel specimens in RA position 12 are predicted to have burnups ranging from 35.8–38.9 MWd/kg-U at the end of the fourth irradiation cycle, slightly less than the minimum desired burnup of 40 MWd/kg-U listed in Table 1 Linear extrapolation was used to predict burnups after the fourth cycle, and the target in RA position 32 was calculated to reach 76.1–81.4 MWd/kg-U after nine irradiation cycles.

To accelerate design efforts, a series of ANSYS calculations were performed to determine the sensitivity of the fuel sample average temperature and spatial ΔT to the gas gap thickness between the sub-capsule and the target housing, the fuel and nonfuel HGRs as a function of burnup and spatial position, and the thickness of the fuel specimens. The authors ran 850 ANSYS cases in which the gas gap thickness varied from 0.5–0.75 mm, the fuel disk thickness was varied from 0.3–1.0 mm, and target positions and days of irradiation were selected so that the entire range of HGRs and burnups were encountered in the sensitivity analysis. The target fill gas was assumed to be pure helium. These gas gap and fuel thickness ranges were selected based on engineering judgment obtained from previous VXF MiniFuel experiment builds. A Python script was developed to read the entirety of the HFIRCON data and ANSYS sensitivity results and used the scikit-learn module [20] to create a ROM based on surface fit to the data using quadratic regression. Subsequently, the results showed that a helium-argon fill gas mixture and gas gap and fuel specimen thicknesses outside the tested range would be required to obtain fuel specimen average temperatures from 1,000–1,300°C and maintain a spatial ΔT below 100°C all within a single target. Therefore, the ROM was not able to predict a design that met the goals listed in Table 1. However, the ROM was able to give a rough starting point that predicted fuel temperatures within approximately 50°C of the design goals, which could then be iterated in ANSYS to achieve the design goals. Future work will include a wider range of variables in an ANSYS sensitivity analysis to improve the accuracy and usability of a ROM with much less computational cost compared with ANSYS.

A summary of the target designs that met the design goals listed in Table 1 are given in Table 2. The two target designs used the same fuel disk thicknesses and nearly identical gas gap thicknesses, but the RA=12 target required an 80% helium/20% argon fill gas mixture, while the RA=32 target required a 63% helium/37% argon fill gas mixture. Figure 11 shows the predicted temperature distribution in the target internal components for position 12 using HGRs from the end of the fourth irradiation cycle and applying the design parameters listed in Table 2. The maximum HGR experienced over the four irradiation cycles was used in Figure 11 which caused the peak fuel temperature to exceed the design goal. The target designs listed in Table 2 were obtained using HGR and burnup values from the middle of the third irradiation cycle, which are approximate average HGRs for the entire irradiation time.

Table 2. Target design parameters that meet example design goals.

Sub-capsule position	Gas gap thickness (mm) (RA=12)	Gas gap thickness (mm) (RA=32)	Fuel disk thickness (mm) (same values used in both designs)	Design T_{avg} (°C)
1	0.539	0.5	0.25	1,000
2	0.564	0.564	0.275	1,100
3	1.0	1.0	0.3	1,300
4	0.929	0.929	0.3	1,300
5	0.554	0.554	0.275	1,100
6	0.5	0.5	0.25	1,000

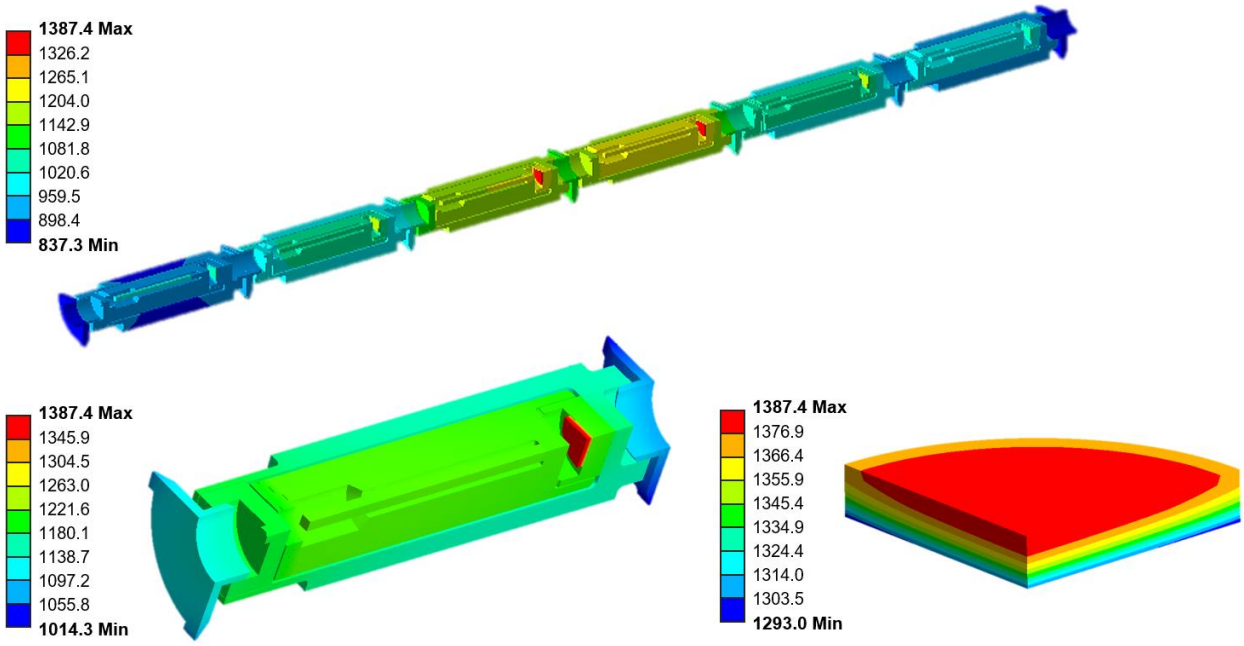

Figure 11. Target internal temperature distributions (in °C) for position RA=12 at EOC 4 showing all sub-capsule positions (*top*), the hottest sub-capsule (*bottom left*), and the fuel specimen in the hottest sub-capsule (*bottom right*).

Figures 12 and 13 show the fuel temperatures predicted for both target designs as a function of time in HFIR (the 26 day irradiation time and 25 day downtime is included for all cycles). Temperatures were calculated using HGRs from the first, second, thirteenth, and twenty-sixth day in each cycle to show how the fuel starts at a relatively low temperature and heats up throughout the cycle. In the figures, markers indicate the average fuel temperature and error bars represent the range from the minimum to maximum spatial fuel temperatures. Figure 14 plots the spatial ΔT within the fuel specimens in target RA position RA=12 as a function of irradiation time. Spatial ΔT predictions within the fuel specimens of target position RA=32 are slightly less than those in target position RA=12 but follow a similar general trend.

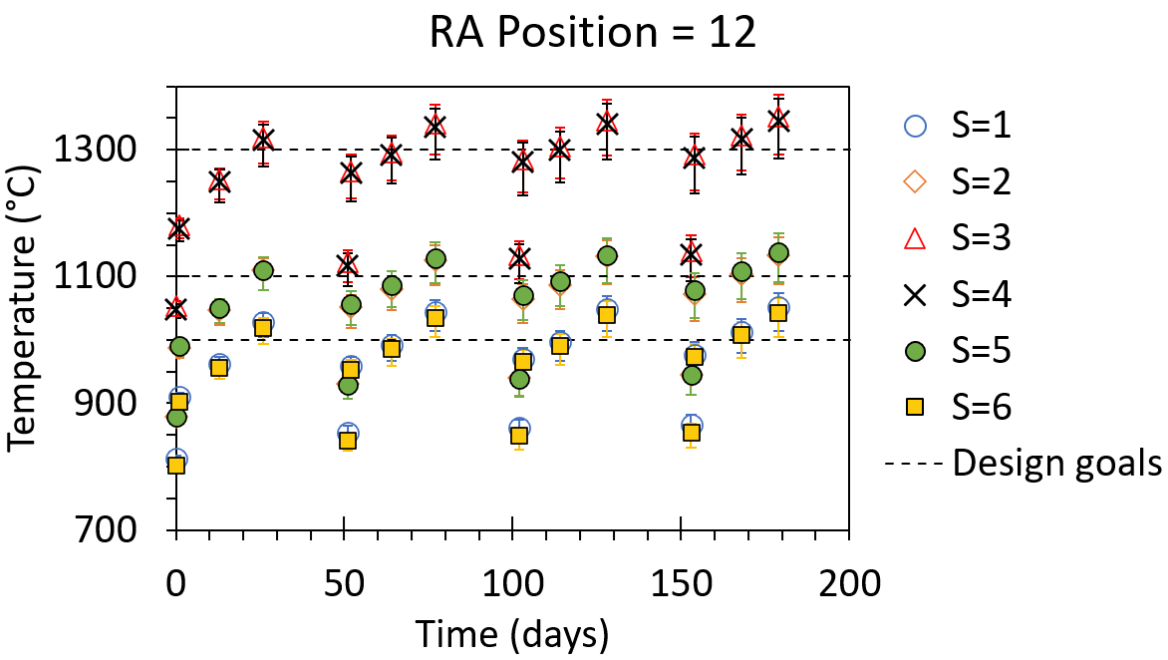

Figure 12. Predicted fuel temperatures in target position RA=12 as a function of irradiation time. Markers represent average values and error bars represent the minimum to maximum range.

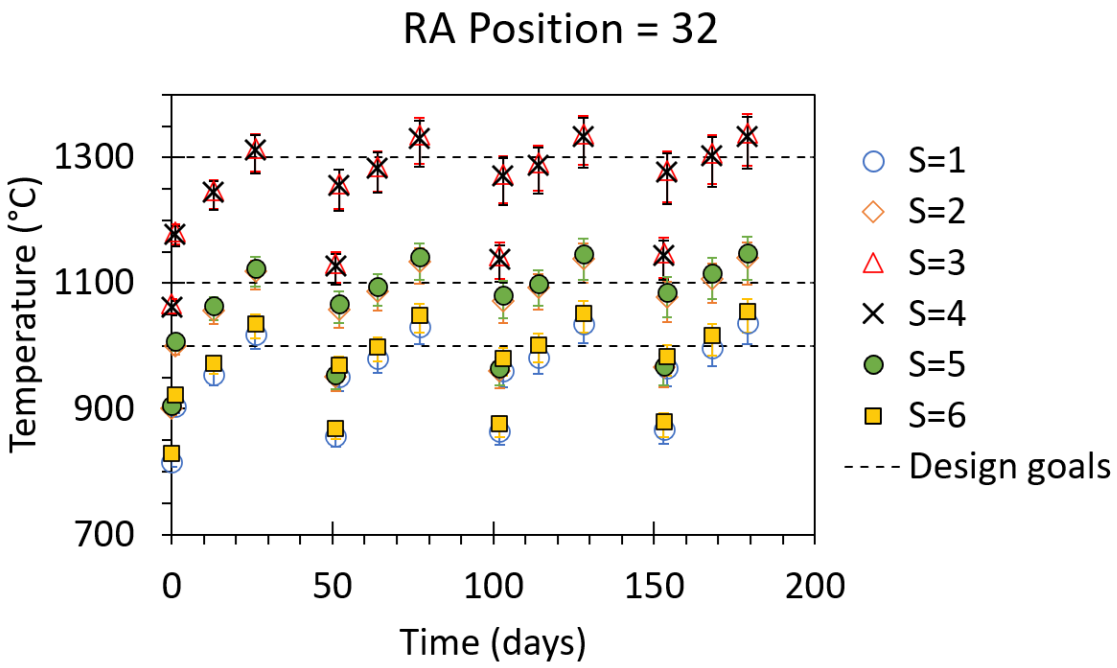

Figure 13. Predicted fuel temperatures in target position RA=32 as a function of irradiation time. Markers represent average values and error bars represent the minimum to maximum range.

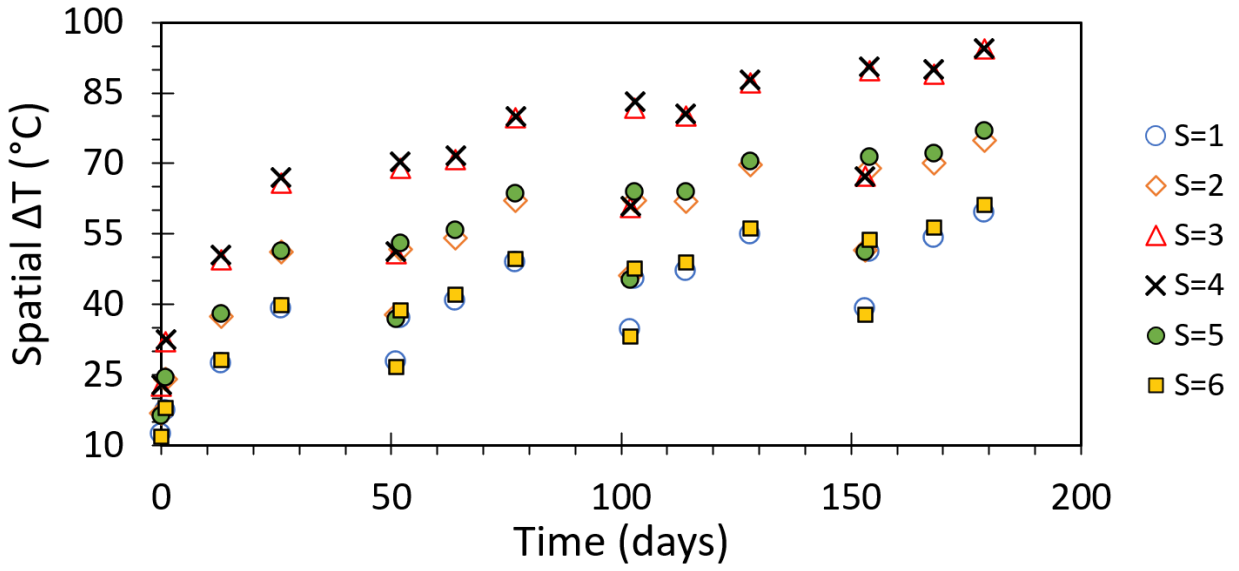

Figure 14. Spatial ΔT in target position 12 as a function of irradiation time. S indicates sub-capsule position.

Figures 12–14 show that the design goals listed in Table 1 can be met while maintaining spatial ΔT values below 100°C for fuel disk thicknesses from 0.25 to 0.3 mm. The maximum spatial ΔT that occurred in positions 12 and 32 were 94.4°C and 83.3°C and occurred in RAS positions 123 and 324, respectively. These maxima both occur on the last day of the fourth irradiation cycle.

The maximum ΔT within a single fuel specimen across all spatial and temporal data points occurred in RAS position 123 and was 348.4°C, meaning that the minimum fuel temperature in the specimen RAS=123 that occurred at any time during the 4 cycle irradiation subtracted from the maximum fuel temperature in that specimen during the 4 cycle irradiation equaled 348.4°C. The minimum ΔT within a single fuel specimen across all spatial and temporal data points occurred in RAS position 321 and was 247.9°C. In each case, roughly half of the temporal ΔT is attributed to the buildup of fission products and plutonium breeding that occurs over the first irradiation cycle and the movement of HFIR's control blades on the first day of each subsequent cycle.

4. SUMMARY AND CONCLUSIONS

This report details an initial MiniFuel design activity for high-temperature irradiation experiments of natural UO_2 in one of HFIR's RB locations. The motivation for this work is the need to accelerate fuel qualification using controlled, separate effects irradiation testing with accelerated burnup accumulation. In the case of UO_2-based fuels, a need also exists to increase irradiation temperatures beyond the limitations of previous irradiation facilities. Neutronics, hydraulics, and FE thermal analyses, complemented by sensitivity analysis methods, were performed to design a pair of MiniFuel targets that met a representative set of design goals. Irradiation in the RB position was shown to achieve HGRs and burnup accumulation rates approximately 2.25 times higher than irradiation experiments previously conducted in HFIR's VXF positions, which are farther from the reactor core. This outcome highlights one of the primary advantages of conducting MiniFuel experiments in the RB region. RELAP5-3D was used to model coolant flow and HTCs through the MiniFuel experiment and showed that the predicted mass flow rate was acceptable, even when the geometry of the design was varied within its dimensional tolerances. The range of HTCs predicted by

RELAP were shown to be inconsequential to fuel temperatures predicted using an FE ANSYS model. ANSYS was used in conjunction with an early-stage ROM developed in Python to design a set of targets that could achieve average fuel temperatures of 1,000°C, 1,100°C, and 1,300°C while maintaining a spatial ΔT below 100°C. The designed targets could be removed from HFIR at the end of irradiation cycles 4 and 9 so that the fuel specimens have burnup values of approximately 36–39 and 78–81 MWd/kg-U. The design temperatures presented in this report were at or above 1,000°C and were obtained by orienting the targets at HFIR's midplane and near the core. Lower temperatures could be achieved if desired in targets above or below the midplane and farther from the core. Future work may determine whether fuel temperature variation greater than 1000–1300°C is achievable within a single target. Engineering drawings of the modified RB basket and targets have been compiled, and future design activities will focus on program- and vendor-specific goals.

5. REFERENCES

[1] D. C. Crawford, D. L. Porter, S. L. Hayes, M. K. Meyer, D. A. Petti and K. Pasamehmetoglu, "An Approach to Fuel Development and Qualification," *Journal of Nuclear Materials,* vol. 371, pp. 232-242, 2007.

[2] K. A. Terrani, N. A. Capps, M. J. Kerr, C. A. Back, A. T. Nelson, B. D. Wirth, S. L. Hayes and C. R. Stanek, "Accelerating Nuclear Fuel Development and Qualification: Modeling and Simulation Integrated with Separate-Effects Testing," *Journal of Nuclear Materials,* vol. 539, p. 152267, 2020.

[3] C. M. Petrie, J. R. Burns, A. M. Raftery, A. T. Nelson and K. A. Terrani, "Separate Effects Irradiation Testing of Miniature Fuel Specimens," *Journal of Nuclear Materials,* vol. 526, p. 151783, 2019.

[4] J. M. Harp, R. N. Morris, C. M. Petrie, J. R. Burns and K. A. Terrani, "Postirradiation Examination from Separate Effects Irradiation Testing of Uranium Nitride Kernels and Coated Particles," *Journal of Nuclear Materials,* vol. 544, p. 152696, 2021.

[5] C. M. Petrie, A. G. Le Coq, M. D. Richardson, C. A. Hobbs, G. W. Helmreich, J. R. Burns and J. M. Harp, "Monolithic ATF MiniFuel Sample Capsules Ready for HFIR Insertion," Oak Ridge National Laboratory, ORNL/SR-2020/4, 2020.

[6] A. G. Le Coq, C. M. Petrie, J. M. Harp, P. Mulligan, P. A. Champlin, N. Russell, K. D. Linton and A. T. Nelson, "FY 2020 AFC HFIR Irradiation and PIE Status Report," Oak Ridge National Laboratory, ORNL/SPR-2020/1731, 2020.

[7] R. C. Gallagher, Z. Wallen, C. M. Petrie, T. Gerczak, A. G. Le Coq, K. Smith, J. Harp, K. D. Linton, B. Collin and R. Latta, "Analysis and Design of High-Power TRISO Fuel Compact Irradiation in HFIR," Oak Ridge National Laboratory, ORNL/TM-2020/1658, 2021.

[8] N. Capps, J. Harp, C. M. Petrie and A. Nelson, "BISON MiniFuel Fission Gas Release Analysis," Oak Ridge National Laboratory, ORNL/TM-2020/1779, 2020.

[9] X-5 Monte Carlo Team, "MCNP - A General Monte Carlo N-Particle Transport Code, Version 5. Volume I: Overview and Theory," Los Alamos National Laboratory, LA-UR-03-1987, 2003.

[10] W. A. Wieselquist, R. A. Lefebvre and M. A. Jessee, Eds., "SCALE Code System, Version 6.2.4," Oak Ridge National Laboratory, ORNL/TM-2005/39, 2020.

[11] S. W. Mosher, A. M. Bevill, S. R. Johnson, A. M. Ibrahim, C. R. Daily, T. M. Evans, J. C. Wagner, J. O. Johnson and R. E. Grove, "ADVANTG - An Automated Variance Reduction Parameter Generator," Oak Ridge National Laboratory, ORNL/TM-2013/416, 2013.

[12] S. C. Wilson, S. M. Mosher, C. R. Daily and D. Chandler, "HFIRCON Version 1.0.5 User Guide," Oak Ridge National Laboratory, ORNL/TM-2020/1742, 2020.

[13] D. Chandler, B. R. Betzler, E. E. Davidson and G. Ilas, "Modeling and Simulation of a High Flux Isotope Reactor Representative Core Model for Updated Performance and Safety Basis Assessments," *Nuclear Engineering and Design,* vol. 366, p. 110752, 2020.

[14] RELAP5-3D Development Team, "RELAP5-3D Code Manuals, Volumes I-V," Idaho National Laboratory, INL/MIS-15-36723, Rev. 4.4, 2018.

[15] Y. A. Çengel and A. J. Ghajar, Heat and Mass Transfer: Fundamentals and Applications, Fifth Edition, New York, NY: McGraw-Hill Education, 2015.

[16] R. Latta, B. Collin, N. Brown, J. Hunn, C. Petrie, T. Gerczak and G. Helmreich, "High Power Irradiation Testing of TRISO Particles in Miniature Fuel Specimens in HFIR," in *Transactions of the American Nuclear Society, Vol. 121*, Washington, D.C., November 17-21, 2019.

[17] R. C. Gallagher, T. Gerczak, G. Helmreich, C. Petrie, Z. Wallen and R. Latta, "Thermal and Neutronic Analyses of High Particle Power TRISO Irradiations using MiniFuel," in *Transactions of the American Nuclear Society*, Virtual Meeting, June 14-16, 2021.

[18] J. L. McDuffee, "Heat Transfer Through Small Moveable Gas Gaps in a Multi-Body System Using the ANSYS Finite Element Software," in *Proceedings of the ASME 2013 Heat Transfer Summer Conference*, Minneapolis, MN, 2013.

[19] Idaho National Engineering Laboratory, "SCDAP/RELAP5/MOD 3.1 Code Manual: MATPRO—A Library of Materials Properties for Light-Water-Reactor Accident Analysis," U.S. Nuclear Regulatory Commission, NUREG/CR-6150, EGG-2720 Vol. 4, 1993.

[20] Pacific Northwest National Laboratory, "FRAPCON-3 Updates, Including Mixed-Oxide Fuel Properties," U.S. Nuclear Regulatory Commission, NUREG/CR-6534, Vol. 4, PNNL-11513, 2005.

[21] F. Pedregosa, G. Varoquaux, A. Gramfort, B. Thirion, O. Grisel, M. Blondel, A. Müller, J. Nothman, G. Louppe, P. Prettenhofer, R. Weiss, V. Dubourg, J. Vanderplas, A. Passos, D. Cournapeau, M. Brucher, M. Perrot and E. Duchesnay, "Scikit-learn: Machine Learning in Python," *Journal of Machine Learning,* vol. 12, pp. 2825-2830, 2011.